# Localized and stationary dynamic gratings via stimulated Brillouin scattering with phase modulated pumps

**Y. Antman,[1] N. Primerov,[2] J. Sancho,[2,3] L. Thevenaz,[2] and A. Zadok[1,*]**

[1]*Faculty of Engineering, Bar-Ilan University, Ramat-Gan 52900 Israel*
[2]*Ecole Polytechnique Fédérale de Lausanne, Institute of Electrical Engineering, SCI-STI-LT Station 11, 1015 Lausanne, Switzerland*
[3]*Permanent address: iTEAM Institute, Universidad Politécnica de Valencia, 46022 Valencia, Spain*
[*] *Avinoam.Zadok@biu.ac.il*

**Abstract:** A novel technique for the localization of stimulated Brillouin scattering (SBS) interaction is proposed, analyzed and demonstrated experimentally. The method relies on the phase modulation of two counter-propagating optical waves by a common pseudo-random bit sequence (PRBS), these waves being spectrally detuned by the Brillouin frequency shift. The PRBS symbol duration is much shorter than the acoustic lifetime. The interference between the two modulated waves gives rise to an acoustic grating that is confined to narrow correlation peaks, as short as 1.7 cm. The separation between neighboring peaks, which is governed by the PRBS length, can be made arbitrarily long. The method is demonstrated in the generation and applications of *dynamic gratings* in polarization maintaining (PM) fibers. Localized and stationary acoustic gratings are induced by two phase modulated pumps that are polarized along one principal axis of the PM fiber, and interrogated by a third, readout wave which is polarized along the orthogonal axis. Using the proposed technique, we demonstrate the variable delay of 1 ns-long readout pulses by as much as 770 ns. Noise due to reflections from residual off-peak gratings and its implications on the potential variable delay of optical communication data are discussed. The method is equally applicable to the modulation of pump and probe waves in SBS over standard fibers.

©2012 Optical Society of America

**OCIS codes:** (060.2310) Fiber optics; (070.1170) Analog optical signal processing; (290.5900) Scattering, stimulated Brillouin; (060.4370) Nonlinear optics, fibers.

## References and links

1.  R. W. Boyd, *Nonlinear Optics,* 3rd edition, (Academic Press, 2008).
2.  T. Kurashima, T. Horiguchi, and M. Tateda, "Distributed-temperature sensing using stimulated Brillouin scattering in optical silica fibers," Opt. Lett. **15**(18), 1038–1040 (1990).
3.  T. Horiguchi, T. Kurashima, and M. Tateda, "A technique to measure distributed strain in optical fibers," IEEE Photon. Technol. Lett. **2**(5), 352–354 (1990).
4.  X. Bao, D. J. Webb, and D. A. Jackson, "22-km distributed temperature sensor using Brillouin gain in an optical fiber," Opt. Lett. **18**(7), 552–554 (1993).
5.  M. Niklès, L. Thévenaz, and P. A. Robert, "Simple distributed fiber sensor based on Brillouin gain spectrum analysis," Opt. Lett. **21**(10), 758–760 (1996).
6.  T. Horiguchi and M. Tateda, "Optical-fiber-attenuation investigation using stimulated Brillouin scattering between a pulse and a continuous wave," Opt. Lett. **14**(8), 408–410 (1989).
7.  A. Fellay, L. Thevenaz, M. Facchini, M. Nikles, and P. Robert, "Distributing sensing using stimulated Brillouin scattering: Toward ultimate resolution," in *Proceedings of the Optical Fiber Sensors Conference* (OFS-12), 324–327 (1997).
8.  J.-C. Beugnot, M. Tur, S. F. Mafang, and L. Thévenaz, "Distributed Brillouin sensing with sub-meter spatial resolution: modeling and processing," Opt. Express **19**(8), 7381–7397 (2011).

9. X. Bao and L. A. Chen, "Recent progress in brillouin scattering based fiber sensors," Sensors (Basel) **11**(4), 4152–4187 (2011).
10. L. Thévenaz, "Brillouin distributed time-domain sensing in optical fibers: state of the art and perspectives," Front. Optoelectron. China **3**(1), 13–21 (2010).
11. K. Hotate and T. Hasegawa, "Measurement of Brillouin gain spectrum distribution along an optical fiber using a correlation-based technique – proposal, experiment and simulation," IEICE Trans. Electron, E **83-C**, 405–412 (2000).
12. K. Hotate and M. Tanaka, "Distributed fiber Brillouin strain Sensing with 1-cm spatial resolution by correlation-based continuous-wave technique," IEEE Photon. Technol. Lett. **14**(2), 179–181 (2002).
13. K. Y. Song, W. Zou, Z. He, and K. Hotate, "All-optical dynamic grating generation based on Brillouin scattering in polarization-maintaining fiber," Opt. Lett. **33**(9), 926–928 (2008).
14. Y. Dong, X. Bao, and L. Chen, "Distributed temperature sensing based on birefringence effect on transient Brillouin grating in a polarization-maintaining photonic crystal fiber," Opt. Lett. **34**(17), 2590–2592 (2009).
15. Y. Dong, L. Chen, and X. Bao, "Truly distributed birefringence measurement of polarization-maintaining fibers based on transient Brillouin grating," Opt. Lett. **35**(2), 193–195 (2010).
16. W. Zou, Z. He, and K. Hotate, "Complete discrimination of strain and temperature using Brillouin frequency shift and birefringence in a polarization-maintaining fiber," Opt. Express **17**(3), 1248–1255 (2009).
17. W. Zou, Z. He, K. Y. Song, and K. Hotate, "Correlation-based distributed measurement of a dynamic grating spectrum generated in stimulated Brillouin scattering in a polarization-maintaining optical fiber," Opt. Lett. **34**(7), 1126–1128 (2009).
18. K. Y. Song, K. Lee, and S. B. Lee, "Tunable optical delays based on Brillouin dynamic grating in optical fibers," Opt. Express **17**(12), 10344–10349 (2009).
19. Y. Dong, L. Chen, and X. Bao, "High-spatial-resolution simultaneous strain and temperature sensor using Brillouin scattering and birefringence in a polarization-maintaining fibre," IEEE Photon. Technol. Lett. **22**(18), 1364–1366 (2010).
20. K. Y. Song, S. Chin, N. Primerov, and L. Thevenaz, "Time-domain distributed fiber sensor with 1 cm spatial resolution based on Brillouin dynamic grating," J. Lightwave Technol. **28**(14), 2062–2067 (2010).
21. K. Y. Song and H. J. Yoon, "High-resolution Brillouin optical time domain analysis based on Brillouin dynamic grating," Opt. Lett. **35**(1), 52–54 (2010).
22. K. Y. Song and H. J. Yoon, "Observation of narrowband intrinsic spectra of Brillouin dynamic gratings," Opt. Lett. **35**(17), 2958–2960 (2010).
23. Y. Dong, L. Chen, and X. Bao, "Characterization of the Brillouin grating spectra in a polarization-maintaining fiber," Opt. Express **18**(18), 18960–18967 (2010).
24. S. Chin, N. Primerov, and L. Thevenaz, "Sub-centimeter spatial resolution in distributed fiber sensing based on dynamic Brillouin grating in optical fibers," IEEE Sens. J. **12**(1), 189–194 (2012).
25. S. Chin, N. Primerov, and L. Thevenaz, "Photonic delay line for broadband optical signals, based on dynamic grating reflectors in fibers," 2010 36th European Conference and Exhibition on Optical Communication - (ECOC 2010), Torino, Italy, (2010).
26. L. Thevenaz, "Slow and fast light in optical fibers," Nat. Photonics **2**(8), 474–481 (2008).
27. A. Zadok, A. Eyal, and M. Tur, "Stimulated Brillouin scattering slow light in optical fibers," Appl. Opt. **50**(25), E38–E49 (2011).
28. Z. Zhu, D. J. Gauthier, Y. Okawachi, J. E. Sharping, A. L. Gaeta, R. W. Boyd, and A. E. Willner, "Numerical study of all-optical slow light delays via stimulated Brillouin scattering in an optical fiber," J. Opt. Soc. Am. B **22**(11), 2378–2384 (2005).
29. J. B. Khurgin, "Performance limits of delay lines based on optical amplifiers," Opt. Lett. **31**(7), 948–950 (2006).
30. R. W. Boyd and P. Narum, "Slow- and fast-light: fundamental limitations," J. Mod. Opt. **54**(16-17), 2403–2411 (2007).
31. M. Santagiustina, and L. Ursini, "Localized Dynamic Brillouin Gratings Permanently Induced by Chaotic Signals," in Signal Processing in Photonic Communications, OSA Technical Digest (CD) (Optical Society of America, 2011), paper JTuB6.
32. T. Erdogan, "Fiber grating spectra," J. Lightwave Technol. **15**(8), 1277–1294 (1997).
33. J. Capmany, B. Ortega, D. Pastor, and S. Sales, "Discrete-time optical processing of microwave signals," J. Lightwave Technol. **23**(2), 702–723 (2005).

## 1. Introduction

Stimulated Brillouin scattering (SBS) requires the lowest activation power of all non-linear propagation effects in standard optical fibers. SBS is driven by the interference between two counter-propagating optical waves that are detuned in frequency. The intensity of the two waves added together includes a slowly-traveling beating term, whose frequency $\Omega$ equals the difference between the frequencies of the two optical waves. The intensity wave introduces traveling variations in the fiber material density, namely an acoustic wave, through electrostriction [1]. The acoustic wave, in turn, is accompanied by a traveling grating of

refractive index variations, due to the photo-elastic effect [1]. The traveling grating can induce a coupling between the two optical waves. Effective coupling, however, requires a strict phase matching that is fulfilled when the frequency difference $\Omega$ closely matches the *Brillouin frequency shift* $\Omega_B$ of the fiber [1], which is on the order of $2\pi \cdot 11$ GHz in standard fibers at telecommunication wavelengths. When the matching condition is met, the velocity of the propagating optical interference pattern equals the speed of sound in the fiber. The relatively long lifetime $\tau \sim 6$ ns of the acoustic wave decrees that $\Omega$ must fall within a few tens of MHz from $\Omega_B$ for efficient SBS to occur. SBS is observed in standard fibers for optical power levels as low as a few mW.

SBS has found practical and commercial application in distributed sensing along standard fibers that are attached to a structure under test [2–5]. Sensing is based on monitoring the local value of the Brillouin frequency shift, which varies with both temperature and mechanical strain [2–5]. In Brillouin optical time domain analysis (B-OTDA), an intense *pump wave* is used to amplify counter-propagating, typically weaker *probe waves* [6]. The position-dependent $\Omega_B$ is recovered through mapping the power of the amplified probe, as a function of both time and frequency detuning $\Omega$. The measurement range of a standard B-OTDA can reach tens of km, however its spatial resolution is fundamentally restricted to the order of 1 m by the acoustic lifetime: The use of either pump or probe pulses much shorter than $\tau$ leads to SBS amplification that is both weaker and spectrally broadened [7]. Recent, more advanced B-OTDA techniques rely on elaborate, multiple pulse patterns and multiple scans to provide an order-of-magnitude higher resolution, at the cost of added complexity (see [8] for a detailed analysis and [9, 10] for a recent review, and references therein).

Due to the inherent limitations of pulsed-mode SBS, extensive research efforts have been dedicated to the generation of SBS interactions that are *both stationary and localized*, starting in the late 1990s. In one scheme, known as Brillouin optical correlation-domain analysis (B-OCDA), the instantaneous frequencies of constant-magnitude pump and probe waves, that are nominally detuned by $\Omega$, are synchronously modulated by a common sine wave [11, 12]. Due to the modulation, the frequency difference between the two counter-propagating waves remains stationary at particular fiber locations only, known as *correlation peaks*, whereas the frequency difference elsewhere is oscillating [11, 12]. Consequently, effective SBS amplification is restricted to the correlation peaks, and probe power measurements may convey localized information. The unambiguous measurement range of B-OCDA, however, is restricted to the separation between periodic correlation peaks, which is typically several hundreds times the spatial resolution. Hence when simple sine-wave frequency modulation is used, tight trade-offs prevail between the B-OCDA range and resolution [11, 12].

In this work, we propose, demonstrate and apply a novel technique for the generation of an SBS interaction that is both localized and stationary. The method relies on the phase modulation of the two waves by a common pseudo-random bit sequence (PRBS), with a symbol duration $T$ that is much shorter than $\tau$. Similar to the B-OCDA technique, the method allows for an effective SBS interaction in discrete, cm-scale correlation peaks only. However, unlike B-OCDA, the separation between neighboring correlation peaks is governed by the length of the PRBS. The unambiguous measurement range can therefore be made arbitrarily long, and it is decorrelated to a wide extent from the spatial resolution.

The proposed method is experimentally demonstrated in the localization of *dynamic SBS gratings* in polarization maintaining (PM) fibers [13–25]. Dynamic gratings are introduced by two counter-propagating pump waves, separated in frequency by $\Omega_B$ and co-polarized along one principal axis of the PM fiber. The SBS interaction between the two pumps introduces a grating of refractive index variations, which can be switched on and off and even moved along the fiber, depending on the profiles of the pump waves. The dynamic grating is interrogated by a third, probe signal, which is polarized along the orthogonal principal axis of the PM fiber. Due to the relatively large birefringence of such fibers, the frequency of the reading signal must be detuned from those of the pumps, typically by a few tens of GHz [13].

The reading signal is back-reflected by the dynamic grating into a fourth wave, which can be measured to monitor the entire process.

Dynamic gratings have been drawing increasing interest, for their considerable potential performance enhancements of SBS applications. The use of a third and fourth optical frequencies in the readout process improves the signal to noise ratio of the measurements. The spectral offset between the pump and readout waves varies with the PM fiber birefringence, which in turn depends on both temperature and strain. Dynamic gratings therefore add another dimension to B-OTDA sensing [14–17, 19–21, 24]: a change in strain or temperature modifies the readout probe frequency of maximum reflection, as well as the value of $\Omega_B$. In addition, dynamic gratings may provide 'movable mirrors', thereby introducing a new potential platform for all-optical variable group delay [18, 25]. Dynamic gratings-based delay could be free of the delay-bandwidth product limitations that undermine the performance of so-called *SBS slow-light* systems [26–30].

When two continuous wave (CW) pumps are used, a uniform dynamic grating is introduced along the entire PM fiber. Localized dynamic gratings have been generated using pump pulses [19, 25]. However, much like B-OTDA measurements over standard fibers, the generation of short gratings is restricted by the acoustic lifetime $\tau$. In addition, the gratings must be 'refreshed' by periodic pump pulses every $\tau$, hence the strength of reflection is temporally varying. B-OCDA was also introduced to obtain localized dynamic gratings [17]. However, the frequency modulation of the two pumps introduces additional complexity, as the readout probe signal must be synchronously modulated as well [17].

In the following, we experimentally demonstrate the generation of cm-scale, stationary and localized dynamic gratings over PM fibers of up to 100 m in length, using PRBS phase modulation of both pumps [31]. In contrast to B-OCDA over PM fibers, no modulation of the readout probe wave is necessary. The gratings are applied to the variable delay of periodic 1 ns-long pulses, by up to 770 ns. The results illustrate the potential impact of the proposed technique on various applications of dynamic gratings. In particular, PRBS-driven gratings could allow for the distributed sensing of temperature and strain using CW readout waves and low-bandwidth detectors. Such sensing experiments are beyond the scope of this paper, and will be reported elsewhere. Lastly, the method is equally applicable to the generation of a localized SBS interaction over standard fibers.

The remainder of this paper is organized as follows. The principle of operation of PRBS-driven, localized and stationary dynamic gratings is explained in section 2, alongside numerical simulations of the spatio-temporal grating profile. The experimental setup is described in section 3. Experimental results of variable delay are provided in sections 4. Finally, the extent of noise due to reflections from residual correlation sidelobes is addressed in section 5. The noise power is quantified in analysis and simulations, and implications on the potential variable delay of real-time optical communication data are discussed. Concluding remarks are given in section 6.

## 2. Brillouin dynamic gratings driven by phase modulated pumps

Let us denote the optical fields of the two pump waves of an SBS dynamic grating as $E_{1,2}(t,z)$, respectively, where $t$ stands for time and $z$ represents position along a PM fiber of length $L$. Pump $E_1$ enters the fiber at $z = 0$ and propagates along the positive $z$ direction, whereas pump $E_2$ propagates from $z = L$ in the negative $z$ direction. The optical frequencies of the two pump waves, $\omega_{1,2}$, are separated by $\Omega$ which is on the order of $\Omega_B$ in the fiber. The complex envelopes of the two waves are denoted by $A_{1,2}(t,z)$, so that:

$$E_1(t,z) = A_1(t,z)\exp(j\omega_1 t) + c.c., \tag{1}$$

$$E_2(t,z) = A_2(t,z)\exp\left[j(\omega_1 + \Omega)t\right] + c.c. \tag{2}$$

In our proposed scheme for generating stationary and localized gratings, the phases of both pump waves are modulated by a common PRBS with symbol duration $T$:

$$A_1(t,z=0) = A_2(t,z=L) = A(t) = A_0\left\{\sum_n \text{rect}\left[(t-nT)/T\right]\exp(j\varphi_n)\right\}. \tag{3}$$

In Eq. (3), $\varphi_n$ is a random phase variable which equals either 0 or $\pi$, $\text{rect}(\xi)$ equals 1 for $|\xi| < 0.5$ and zero elsewhere, and $A_0$ denotes the constant magnitude of both pump waves. In the following, we consider both pumps to be of the same power, for simplicity. The analysis is equally valid for pumps having different power levels. The modulation is synchronized so that the phases of the two pumps, at their respective entry points into the fiber, are equal for all $t$. Both pumps are polarized along the same principal axis of the PM fiber, denoted as $\hat{\mathbf{x}}$.

Consider next the magnitude of the acoustic density wave of frequency $\Omega$ that is generated by the two pumps. Since the acoustic velocity is orders of magnitude slower than the speed of light, the acoustic wave, generated by the optical pump waves at a given $z$, can be regarded as a local, time-dependent but non-propagating disturbance [1, 8]. The temporal evolution of the density wave magnitude is governed by the following equation [1, 8]:

$$\frac{\partial Q(t,z)}{\partial t} + j\frac{\Omega_B^2(z) - \Omega^2 - j\Omega\Gamma_B}{2\Omega}Q(t,z) = jg_1 A_1(t,z)A_2^*(t,z). \tag{4}$$

In Eq. (4), $\Gamma_B = 1/\tau$ is the SBS linewidth, and the value of the parameter $g_1$ depends on the speed of sound in the fiber, its electrostrictive coefficient and density [8]. Within $\Gamma_B$, $g_1$ can be regarded as constant [1,8]. For brevity, we define the following notation: $\Gamma_A(\Omega,z) \equiv j\left[\left(\Omega_B^2(z) - \Omega^2 - j\Omega\Gamma_B\right)/2\Omega\right]$ [8]. On resonance ($\Omega = \Omega_B$), $\Gamma_A$ reduces to its minimum value of $\frac{1}{2}\Gamma_B$.

In what follows, it is presumed that the pump waves are sufficiently strong, and that the SBS interaction is sufficiently localized, so that the pump waves are undepleted. It is also assumed that spontaneous Brillouin scattering of the phase-modulated pumps is negligible. Subject to these conditions, the solution of Eq. (4) can be formally expressed as:

$$
\begin{aligned}
Q(t,z) &= jg_1\exp(-\Gamma_A t)\int_0^t \exp(\Gamma_A t')A\left(t'-\frac{z}{v_g}\right)A^*\left(t'-\frac{L-z}{v_g}\right)dt' \\
&= jg_1\int_0^t \exp\left[-\Gamma_A(t-t')\right]A\left(t'-\frac{z}{v_g}\right)A^*\left(t'-\frac{L-z}{v_g}\right)dt' \\
&= jg_1\int_0^t \exp\left[-\Gamma_A(t-t')\right]A\left(t'-\frac{z}{v_g}\right)A^*\left[t'-\frac{z}{v_g}-\theta(z)\right]dt'.
\end{aligned}
\tag{5}
$$

The position-dependent temporal offset $\theta(z)$ in Eq. (5) is defined as: $\theta(z) \equiv (2z-L)/v_g$, with $v_g$ the group velocity of light in the fiber. At the limit $t \gg 1/\Gamma_A$, the acoustic wave magnitude becomes proportional to the product $A(t-z/v_g)A^*[t-z/v_g-\theta(z)]$, weighed and summed by a moving exponential window of duration $1/\Gamma_A$. When the pumps modulation $A(t)$ is driven by an ergodic random process, that is fluctuating much faster than $1/\Gamma_A$, the strength of the acoustic wave following its initial buildup provides a measure of the modulation autocorrelation function:

$C(\theta) = \langle A(t) A^* [t - \theta(z)] \rangle$ (with the triangular brackets denoting averaging with respect to $t$).

Referring to our PRBS phase modulation scheme of Eq. (3), we can distinguish between the temporal evolutions of the acoustic dynamic grating in two regions. Within a short section surrounding the center of the fiber at $z = L/2$ the offset $\theta(z)$ is near zero, leading to: $A(t' - z/v_g) A^* [t' - z/v_g - \theta(z)] = |A_0|^2$. The two modulated pump waves are correlated in this particular location, hence the driving force for the acoustic grating generation is stationary and of constant phase. Consequently, the acoustic grating in the vicinity of $z = L/2$ is allowed to build up to its steady state magnitude: $Q(t \gg 1/\Gamma_A, z = L/2) = jg_1 |A_0|^2 / \Gamma_A(\Omega, z = L/2)$. The width of the correlation peak is on the order of $\Delta z = \frac{1}{2} v_g T$, corresponding to the spatial extension of a symbol of the PRBS. In all other $z$ locations, on the other hand, $A(t' - z/v_g) A^* [t' - z/v_g - \theta(z)]$ is randomly alternating between $\pm |A_0|^2$ due to the random phase change between 0 and $\pi$, on every symbol duration $T \ll \tau$. The long term integration thus averages to a zero expectation value and the buildup of the acoustic grating outside the correlation peak is therefore inhibited. The acoustic grating that is generated by PRBS modulation of the pump waves is both stationary and localized. (Note that the strength of the grating outside the correlation peak, however weaker, has a non-zero standard deviation and time varying amplitude. The noise due to scattering from such residual off-peak gratings and its implications are addressed in detail in section 5.)

Similarly to B-OCDA techniques, PRBS phase modulation of the pump waves generates multiple correlation peaks. The separation $Z$ between adjacent peaks equals $\frac{1}{2} M v_g T$, where $M$ is the PRBS length. The correlation peaks, with the exception of the zeroth-order one, can be scanned across a fiber under test through changing the length factor $M$ or the symbol duration $T$. The unambiguous measurement range can be made arbitrarily long with increasing $M$, while retaining the above resolution of $\Delta z$. Since there is no frequency modulation of the pumps the spatial period of the acoustic grating does not oscillate, and the subsequent readout of the acoustic grating by a $\hat{\mathbf{y}}$ polarized interrogating wave becomes considerably simpler than in B-OCDA over PM fibers. The technique is not restricted to dynamic gratings over PM fibers: it is equally applicable to the modulation of pump and probe waves interacting along a standard fiber.
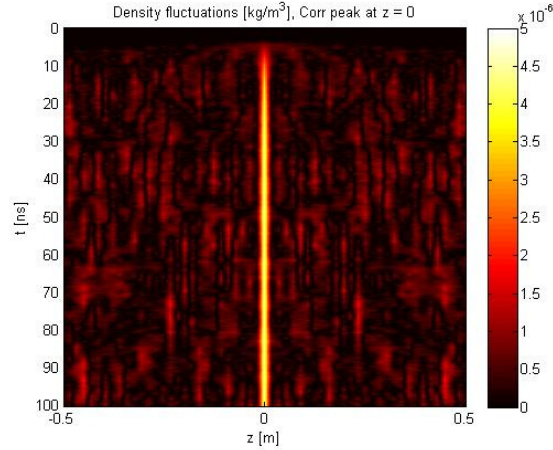
Fig. 1. Simulated magnitude of the acoustic wave density fluctuations, (in kg/m$^3$), that is generated by two pumps, which are phase-modulated by a common pseudo-random bit sequence, as a function of position $z$ and time $t$ within a 1 m-long fiber. The frequency separation between the two pumps was chosen to match the Brillouin frequency shift in the fiber. The modulation symbol rate $T$ was 200 ps.

Figure 1 shows simulation results of the acoustic grating magnitude, as a function of time and position, within a 1 m long fiber. The gratings magnitude was calculated through direct integration of Eq. (4), subject to the PRBS modulation of the pumps phases as in Eq. (3) with $T = 200$ ps. The frequency shift $\Omega$ between the two modulated pumps was chosen to match $\Omega_B$ of the fiber. The simulation predicts the build-up of a localized and stationary grating in a narrow region at the center of fiber, as suggested by the above considerations. The experimental realization of such gratings is presented next. For the sake of generality, the quantity $\left|A_0\right|^2$ may be simply replaced by $A_{01}A_{02}^*$ in all final expressions if the interacting waves have different amplitudes.

## 3. Experimental setup

Figure 2 illustrates the experimental setup that was used for the generation and characterization of dynamic acoustic gratings, driven by random phase modulation of both pump waves. A single distributed feed-back (DFB) laser diode of frequency $\omega_1$ was used to generate both pump waves. The output of the pumps DFB was modulated by an electro-optic phase modulator (EOM), which was driven by a PRBS generator. The output peak-to-peak voltage of the PRBS generator was adjusted to match $V_\pi$ of the EOM (~3.7V), and its clock rate was controlled by a microwave generator. The modulated DFB light was split in two arms. Light in one path was amplified by an erbium-doped fiber amplifier (EDFA) to $\left|A_1\right|^2$ ~200 mW, polarized along the $\hat{\mathbf{x}}$ principal axis of a PM fiber, and launched into a section of specialty PM fiber under test (FUT) as pump 1. Light in the other arm was modulated by a second EOM, which was driven by a sine wave of frequency $\Omega$ ~$2\pi\cdot10$ GHz from a second microwave generator. The EOM in this arm was biased to suppress the optical carrier at $\omega_1$. The upper modulation sideband of frequency $\omega_2 = \omega_1 + \Omega$ was selected by a narrow-band fiber Bragg grating (FBG), amplified by a second EDFA to $\left|A_2\right|^2$ ~200 mW, and launched along the $\hat{\mathbf{x}}$ axis from the opposite end of the FUT as pump 2. The residual carrier wave and the other modulation sideband of pump 2 were rejected by the FBG.
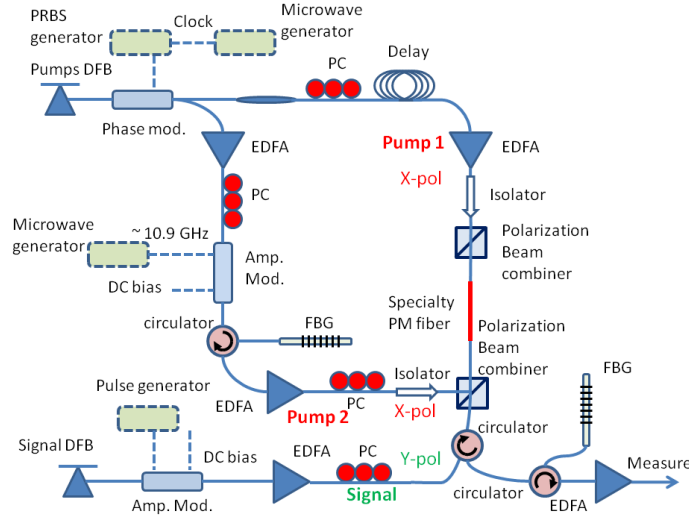
Fig. 2. Experimental setup for the generation and characterization of dynamic acoustic gratings, using SBS with phase-modulated pump waves. PC: polarization controller.

Light from a second DFB laser was used to generate the readout signal wave. The optical frequency of the signal DFB was adjusted via temperature and current control to match the frequency $\omega_{sig}$ of maximum reflectivity of the acoustic dynamic grating along the $\hat{\mathbf{y}}$ principal axis [13]:

$$\omega_{sig} = \omega_2 + \Delta\omega = \omega_2 - \frac{\Delta n}{n_y^g + (n_y^g - n_y)\dfrac{\Delta n}{n_y^g}}\omega_2 \approx \omega_2 - \frac{\Delta n}{n_y^g}\omega_2. \tag{6}$$

In Eq. (6), $\Delta n \ll 1$ is the birefringence, i.e. the difference between the indices of refraction $n_x$ and $n_y$ along $\hat{\mathbf{x}}$ and $\hat{\mathbf{y}}$ axes, and $n_y^g$ denotes the group index along $\hat{\mathbf{y}}$ axis. In Eq. (6), the right term in the denominator is normally $10^{-6}$ smaller than $n_y^g$ in standard PM fibers, so that it can be neglected in most situations and has not yet been explicitly expressed [15]. In the FUTs used in our experiments, $\Delta n$ was on the order of $-5 \cdot 10^{-4}$, corresponding to $\Delta\omega \sim 2\pi \cdot 80$ GHz. Some of the measurements relied on continuous wave readout signals, whereas in other experiments a third EOM was used to generate readout pulses or sine-wave modulation, as necessary. The readout signal wave was polarized along the $\hat{\mathbf{y}}$ principal axis of the PM FUT, and was launched to probe the acoustic dynamic grating. The reflected signal of frequency $\omega_{read} = \omega_1 + \Delta\omega$ was filtered by another FBG, amplified and measured using either a low-bandwidth or a high-bandwidth detector, depending on the specific experiment. Figure 3 provides a schematic illustration of the respective frequencies and directions of propagation of the four optical waves.
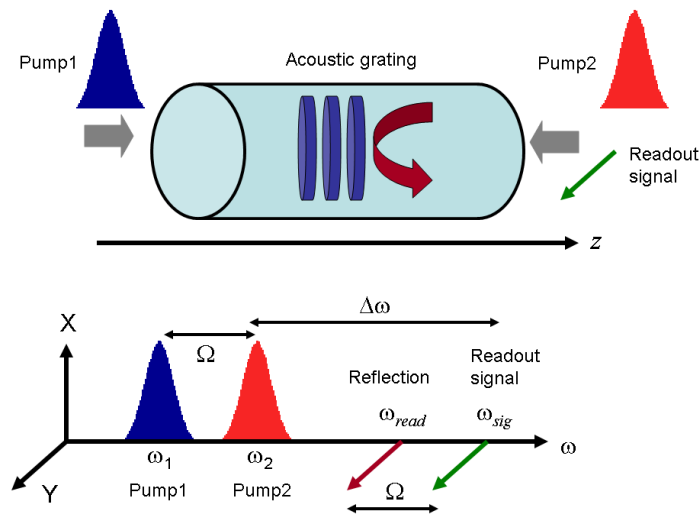
Fig. 3. Schematic illustration of the relative frequencies, states of polarization and directions of propagations for the two pump waves, readout signal and reflection in a dynamic acoustic grating measurement.

## 4. Experimental results: localized and stationary dynamic SBS gratings

The localization of the dynamic gratings was demonstrated using periodic, isolated readout pulses that were 260 psec long. Figure 4 shows the detected power of the reflected signal pulses as a function of time. Maximum reflectivity was achieved for $\Omega = \Omega_B = 2\pi \cdot 10.318$ GHz and $\Delta\omega = 2\pi \cdot 84$ GHz. When CW pumps were used (PRBS generator switched off), a distributed reflection of the readout pulses was observed, with a duration of $2L/v_g$ ~10 ns (see curve 4(a)). The distributed reflection suggests that an extended, nearly uniform dynamic grating had been generated along the entire length of the FUT, the amplitude change being simply accounted to a fluctuating birefringence. Curves 4(b) and 4(c) show the temporal profiles of the reflected readout pulses with the PRBS phase modulation of the pump waves switched on, using $T = 1$ ns and 167 ps, respectively. A reflection from a localized dynamic grating is evident. The power reflectivity of the shorter grating written with $T = 167$ ps is $-37$ dB. It is weaker than that of the longer grating, as expected. All traces in Fig. 4 were averaged over 20 repetitions of the readout pulses. Figure 5 compares the temporal profile of the input pulse power and that of the reflected pulse, using $T = 167$ ps. The full width at half maximum of the reflected pulses was broadened by 40%, fully consistent with an integrated reflection over the grating length.
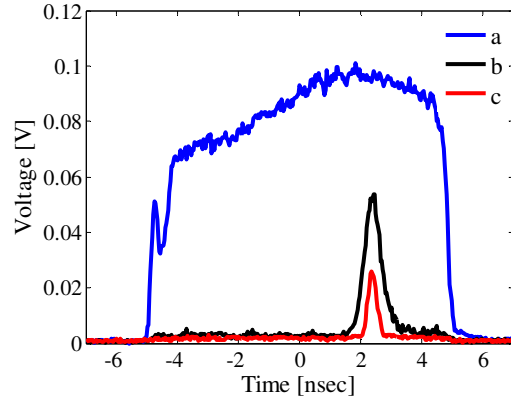
Fig. 4. Reflected waveforms from dynamic acoustic gratings, interrogated with 260 ps long, isolated periodic readout pulses. a) – Grating written by continuous wave pumps. b) The phases of both pump waves was modulated by a PRBS, $T = 1$ ns. c) Same as b), $T = 167$ ps.
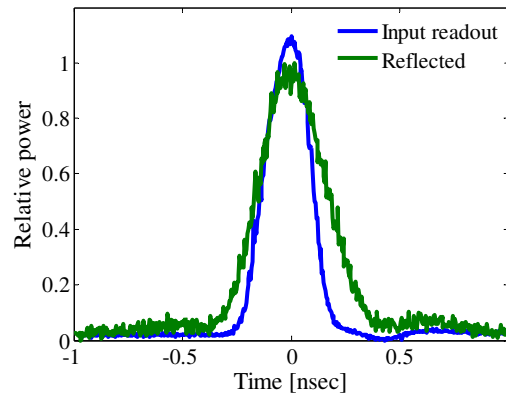


Fig. 5. Temporal profile of the readout pulses at the input of the fiber under test, and following reflection from a dynamic grating generated by phase-modulated pumps, $T = 167$ ps.

The variable delay of isolated readout pulses was demonstrated along a 100 m long FUT ($\Omega_B = 2\pi \cdot 10.87$ GHz, $\Delta\omega = 2\pi \cdot 57$ GHz). In this experiment, a PRBS of length $M = 2^{10} - 1$ was used in the modulation of both pumps, and a fiber delay imbalance was added to the path of pump 1 so that the 10th correlation peak was scanned along the FUT. Figure 6 shows the relative delay of reflected pulses, using seven different symbol durations $T$. A variable delay of 770 ns, or 770 times the temporal width of the readout pulses, is readily observed. (The right-most peak in Fig. 6 is due to a parasitic reflection at frequency $\omega_{sig}$ that was not filtered out.) Fine tuning of the variable delay on a sub-ns scale is shown in Fig. 7.
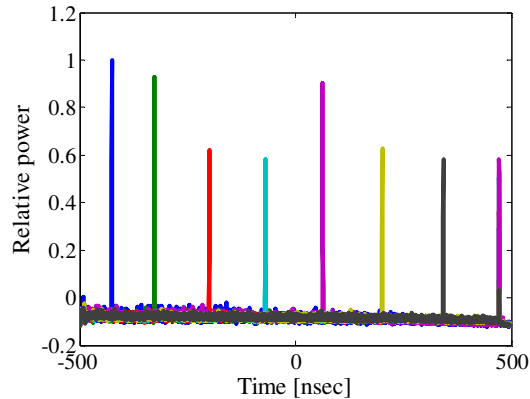
Fig. 6. Variable delay of reflected isolated and periodic readout pulses. The pulses were reflected from dynamic gratings, introduced by the 10th correlation peak of phase-modulated pump waves. The PRBS modulation clock rates $1/T$ were (left to right): 1.120 GHz, 1.108 GHz, 1.093 GHz, 1.078 GHz, 1.063 GHz, 1.048 GHz, 1.033 GHz. (The right-most peak, which is common to all PRBS rates, is due to a parasitic reflection.)
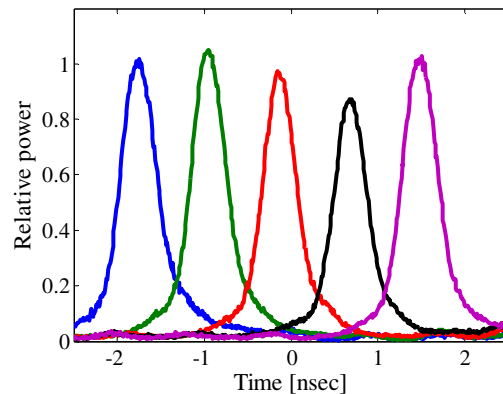


Fig. 7. Variable delay of reflected isolated and periodic readout pulses. The pulses were reflected from dynamic gratings, introduced by the 10th correlation peak of phase-modulated pump waves. The PRBS modulation clock rate $1/T$ for the right-most peak was 1.118670 GHz. The clock rate was raised by 100 kHz, 200 kHz, 300 kHz and 400 kHz for the second through fifth peaks from the right, respectively.

The frequency response of the dynamic gratings reflections was characterized using a vector network analyzer (VNA). An EOM in the readout signal path was driven by a swept sine-wave from the VNA output port, and the detected reflection was analyzed using the input port of the instrument. Figure 8 shows the relative transfer function of the reflected signal power, as a function of the offset of the readout frequency from $\omega_{sig}$ of maximum reflectivity.

Since the acoustic grating magnitude is related to the auto-correlation of the modulating sequence (see Eq. (5)), we expect that frequency response to be connected with the power spectral density of the sequence squared. Note, however, that the relation is not exact due to the temporal windowing that is involved in the inertial generation of the grating. As expected, the reflectivity response broadens with an increase of the PRBS rate, as the dynamic grating becomes shorter. The bandwidth of readout signals that can be accommodated by the dynamic gratings is on the order of the clock rate of the PRBS pump modulation. The relatively high reflectivity at the low frequencies (offset < 200 MHz) is due to a residual extended grating, spanning over the entire length of the FUT: the CW components of the pump waves could not

be entirely suppressed due to a driving voltage on the phase EOM that did not precisely match its $V_\pi$ value
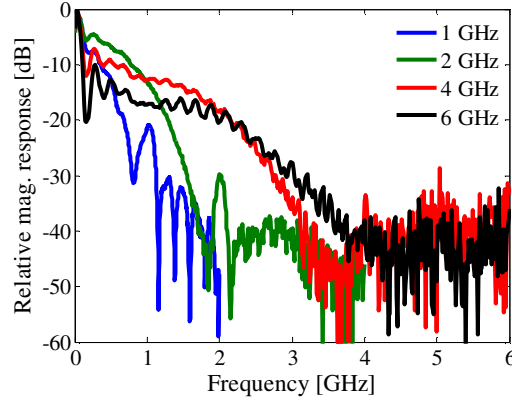


Fig. 8. Vector network analyzer measurements of the power transfer function of the reflections from dynamic gratings. The gratings were generated with phase-modulated pumps, using PRBS with clock rates $1/T$ of 1 GHz. 2 GHz, 4 GHz and 6 GHz.

## 5. Noise due to reflections from correlation sidelobes

So far, we have shown through analysis, simulation and experiments that phase modulation of both pump waves with a high-rate PRBS effectively confines the acoustic dynamic grating to narrow correlation peaks. The acoustic wave magnitude outside the correlation peaks, however weaker, is nonetheless fluctuating and instantaneously nonzero, as can be seen in both Eq. (5) and the simulation results of Fig. 1. In this section, we attempt to quantify the extent of noise due to reflections from such residual gratings, and examine their implications on the potential application of dynamic gratings as variable optical delay lines.

First, let us propose a rather simplistic analytic model for the residual reflections noise in delaying a readout signal sequence. We examine a worst-case scenario in which $\Omega_B$ is constant throughout the entire length of a uniform fiber under test, and adjust $\Omega = \Omega_B$. Consider a fiber section of length $\Delta z = \frac{1}{2} v_g T$ that is outside the correlation peak. We assume that the temporally-varying driving force of the acoustic wave generation, (right-hand side of Eq. (4)), is spatially uniform throughout the short section at all $t$. The driving force is randomly changing between either $jg_1|A_0|^2$ or $-jg_1|A_0|^2$ every $T \ll \tau$, with equal probabilities for both states. The magnitude of the generated acoustic wave is given by an integral over the driving force, weighed by a moving exponential window of duration $2\tau$ (see Eq. (5)). In the simplified model below, we replace the exponential weighing function with a finite and uniform rectangular window, leading to the following approximation of the acoustic density wave magnitude:

$$\tilde{Q}(t,z) \approx jg_1 \int_{t-2\tau}^{t} A(t') A^* [t' - \theta(z)] \, dt'. \tag{7}$$

Subject to the above assumptions and simplifications, the statistics of the acoustic wave magnitude within a short section outside the correlation peak are equivalent to that of a one-dimensional random walk process with a step size of $|r| = Tg_1|A_0|^2$ and a finite number of steps $N_0 = 2\tau/T$. The process is of zero mean value, and its standard deviation equals $\sigma_{\Delta z} = \sqrt{N_0}|r| = \sqrt{2\tau T} g_1|A_0|^2$. The magnitude of the grating at the correlation peak, on the

other hand, is given by Eq. (5): $S = \left| Q\left(t \gg \tau, z = L/2\right) \right| = 2\tau g_1 \left| A_0 \right|^2$. (Recall that the fiber length occupied by the correlation peak is approximately $\Delta z$).

The optical power of the reflected readout signal, for a weak index modulation, is proportional to the magnitude squared of the acoustic grating [1] and its length squared [32]. Hence the intended signal power due to reflection from the correlation peak scales with $\left| S \right|^2 \left(\Delta z\right)^2$. The noise power is accumulated over a large number of sections of length $\Delta z$, each contributing a reflection due to its own residual grating. The number of sections is related to the maximum variable delay $T_D$ of the readout signal: $N = L/\Delta z = T_D/T$ (note that the maximum delay corresponds to two-way propagation over length $L$). In another simplifying assumption, we reasonably suppose that the magnitudes of the gratings in different locations are uncorrelated to one another. When the readout signal to be delayed, for example, is an on-off keying (OOK) data sequence, the noise field consists of the sum of $\frac{1}{2}N$ uncorrelated contributions of equal statistics. The average signal power for OOK data is divided by 2. Altogether, the optical signal to noise ratio (OSNR) predicted by our simplified model is given by:

$$\text{OSNR} = \frac{\frac{1}{2}\left| S \right|^2 \cdot \left(\Delta z\right)^2}{\frac{1}{2}N\sigma_{\Delta z}^2 \cdot \left(\Delta z\right)^2} = \frac{\frac{1}{2}4\tau^2 g_1^2 \left| A_0 \right|^4}{\frac{1}{2}\frac{T_D}{T}2\tau T g_1^2 \left| A_0 \right|^4} = \frac{2\tau}{T_D}. \tag{8}$$

Note that the OSNR predicted by the simplified model is independent of the symbol rate $T$. In the processing of optical communication data, the required OSNR should be at least on the order of 20-30. We therefore conclude that PRBS-driven dynamic gratings cannot delay an incoming data sequence with sufficient OSNR, unless the extent of delay is restricted to a fraction of the acoustic lifetime $\tau$, on the order of 1 ns or less. The noise from residual reflections is of lesser concern in distributed sensing applications, or in the delay of periodic, repetitive patterns, since it can be averaged out (see section 4).

The above approximate model is corroborated by numeric simulations of the reflection OSNR. A pseudo-random OOK data sequence was used as a readout signal. The calculated OSNR values of the simulations and the analytic model for several combinations of $T_D$ and $T$ are provided in Table 1. Even for an FUT as short as 1 m, the OSNR obtained in the simulation is an order of magnitude below the required range of values. As suggested by the model, the OSNR appears to be inversely proportional to $T_D$ and largely independent of $T$. Despite its limitations, the simplified analytic model is seen to provide a useful estimate of the expected OSNR when PRBS-driven dynamic gratings are used as variable optical delay lines.

Table 1. Simulated optical signal to noise ratios for the reflections of on-off keying data from PRBS-driven dynamic gratings. Calculations were made for various fiber lengths *L* and PRBS symbol durations *T*. The acoustic lifetime was taken to be 6 ns. In all simulations, the on-off-keying symbol duration was set to 2*T*, in order to remove the effects of the variable grating bandwidth (see Fig. 8). The results are compared with the optical signal to noise ratios that are predicted by a simplified analytic model.

| | $1/T$ = 1 GHz | $1/T$ = 2 GHz | $1/T$ = 4 GHz | Prediction |
|---|---|---|---|---|
| $L$ = 1 m ($T_D$ = 10 ns) | 2 | 1.65 | 1.75 | 1.2 |
| $L$ = 3 m ($T_D$ = 30 ns) | 0.45 | 0.45 | 0.53 | 0.4 |
| $L$ = 5 m ($T_D$ = 50 ns) | 0.34 | 0.25 | 0.24 | 0.24 |

Improvements to the OSNR might be possible if more elaborate phase coding sequences, rather then pseudo-random bits, are used in the pumps modulation. If, for example, codes are used for which $\sigma_{\Delta z} = \left| r \right| = T g_1 \left| A_0 \right|^2$, the OSNR could improve by a factor of $N_0 \gg 1$ to

$4\tau^2/\left(T_D T\right)$. In this case, coding with a symbol duration of $T$ = 200 ps would allow for a variable delay on the order of 25 ns with sufficient OSNR. As seen in the VNA measurements of section 4, the grating bandwidth can accommodate readout signal pulses whose duration is on the order of $T$. We may therefore expect a variable delay of ~100 bit durations in this case. However, thus far we have been unable to find coding sequences of sufficient length that could provide such low values of $\sigma_{\Delta z}$. The optimization of phase modulation codes is the subject of ongoing work.

## 6. Conclusions

In this work, we have introduced and demonstrated a novel technique for the generation of localized and stationary acoustic gratings. The technique relies on the phase modulation of two optical pump waves by a common, high rate PRBS. The effective generation of the acoustic gratings is confined to discrete correlation peaks. The length of the gratings is governed by PRBS symbol duration rather then the much longer acoustic lifetime. The separation between neighboring peaks, and hence the unambiguous measurement range, can be made arbitrarily long using routine PRBS generation. Localized dynamic gratings had previously been realized using isolated pump pulses. Such gratings are free of off-peak scattering noise, and can be made stronger using intense pulses. However, the inertial generation of pulses-driven gratings that are shorter then tens of cm is limited by the acoustic lifetime τ and prevents the gratings from reaching their full steady-state amplitude. In addition, the magnitude of the gratings decays exponentially, and they must therefore be refreshed every τ. Consequently, the free tuning range of the grating position is restricted to only a few meters. In contrast, using PRBS phase modulation of both pumps, we had experimentally demonstrated the generation of stationary gratings as short as 1.7 cm, separated by as much as 100 meters. The length of the gratings can be reduced below 1 cm with higher modulation rates and their separation extended to the kilometer range using a longer sequence. The power reflectivity of a 1 cm-long grating could reach the order of −30 dB with pump power levels of hundreds of mW. The measurement range would only be limited by the length of practical PM fibers of uniform birefringence.

Although the technique is perfectly applicable to pump-probe SBS interactions along standard fibers, the experimental demonstration of the method had focused on dynamic gratings in PM fibers, enabling a better and unambiguous characterization of the grating properties since the activating and readout signals can be entirely distinct waves, in frequency and polarization. In addition dynamic gratings over PM fibers offer several advantages: the use of a third and fourth optical frequencies improves the measurement signal to noise ratio; the sensitivity of the PM fiber birefringence to both temperature and strain variations adds another dimension to sensing applications; and the need for polarization tracking or scrambling is circumvented.

Perhaps the most intriguing potential application of the PRBS-driven dynamic gratings described in this work is in the all-optical variable delay of reflected readout data. In principle, the gratings provide a 'movable mirror' that can be scanned over paths that are many μs-long, and accommodate signals of several GHz bandwidth. In addition, the wavelength conversion that accompanies the delay is minimal (an offset by the Brillouin shift). Unfortunately, both analysis and simulations show that the accumulative effect of scattering noise from residual gratings spanning the entire length of the fiber is severely restricting the reflection OSNR. The particular pumps coding scheme used in this work, based on a random binary phase sequence, is not optimal in terms of the reflection OSNR. On-going work is focusing on more elaborate coding schemes in attempt to reduce the residual scattering noise. It remains that the technique offers an unprecedented flexibility for applications in which signal averaging is possible, such as the delay of repetitive signals or distributed sensing. Ongoing work is being dedicated to the application of the proposed technique for the

distributed sensing of temperature and strain over standard as well as PM fibers. More advanced configurations are being examined as well, such as microwave-photonic filtering based on reflections from multiple dynamic acoustic gratings [33], or the generation of reflective filters of arbitrary shapes.

## Acknowledgments